ORIGINAL PAPER

CrossMark

Quantification of climatic feedbacks on the Caspian Sea level variability and impacts from the Caspian Sea on the large-scale atmospheric circulation

Klaus Arpe[1] · Ben-Jei Tsuang[2] (ORCID) · Yu-Heng Tseng[3] · Xin-Yu Liu[2] · Suzanne A. G. Leroy[4]

Abstract

With a fall of the Caspian Sea level (CSL), its size gets smaller and therefore the total evaporation over the sea is reduced. With a reduced evaporation from the sea, the fall of the CSL is weakened. This creates a negative feedback as less evaporation leads to less water losses of the Caspian Sea (CS). On the other hand, less evaporation reduces the water in the atmosphere, which may lead to less precipitation in the catchment area of the CS. The two opposite feedbacks are estimated by using an atmospheric climate model coupled with an ocean model only for the CS with different CS sizes while keeping all other forcings like oceanic sea surface temperatures (SSTs) and leaf area index the same from a global climate simulation. The investigation is concentrated on the medieval period because at that time the CSL changed dramatically from about − 30 to − 19 m below the mean ocean sea level, partly man-made. Models used for simulating the last millennium are not able to change the size of the CS dynamically so far. When results from such simulations are used to investigate the CSL variability and its causes, the present study should help to parameterize its feedbacks.

A first assumption that the total evaporation from the CS will vary with the size of the CS (number of grid points representing the sea) is generally confirmed with the model simulations. The decrease of grid points from 15 to 14, 10, 8 or 7 leads to a decrease of evaporation to 96, 77, 70 and 54%. The lower decrease than initially expected from the number of grid points (93, 67, 53 and 47%) is probably due to the fact that there would also be some evaporation at grid points that run dry with a lower CSL but a cooling of the CS SST with increasing CS size in summer may be more important. The reduction of evaporation over the CS means more water for the budget of the whole catchment of the CS (an increase of the CSL) but from the gain through reduced evaporation over the CS, only 70% is found to remain in the water budget of the whole catchment area due to feedbacks with the precipitation. This suggests a high proportion of recycling of water within the CS catchment area.

When using a model which does not have a correct CS size, the effect of a reduced CS area on the water budget for the whole CS catchment can be estimated by taking the evaporation over the sea multiplied by the proportional changed area. However, only 50% of that change is ending up in the water balance of the total catchment of the CS. A formula is provided. This method has been applied to estimate the CSL during the Last Glacial Maximum to be at − 30 to − 33 m.

The experiments show as well that the CS has an impact on the large-scale atmospheric circulation with a widened Aleutian 500 hPa height field trough with increasing CS sizes. It is possible to validate this aspect with observational data.

✉ Ben-Jei Tsuang
   btsuang@gmail.com

[1]   Max Planck Institute for Meteorology, Hamburg, Germany

[2]   Department of Environmental Engineering, Innovation and Development Center of Sustainable Agriculture (IDCSA), National Chung Hsing University, Taichung, Taiwan

[3]   Institute of Oceanography, National Taiwan University, Taipei, Taiwan

[4]   CEREGE, CNRS, IRD, Collège de France, Technopôle de l'Environnement Arbois-Méditerranée, Aix-Marseille University, Aix-en-Provence, France

1 Introduction

The Caspian Sea (CS) is the largest inland body of water on Earth. It is fed by 130 rivers, the most significant being the Volga that enters from the north and accounts for about 80% of the inflowing waters. Today, the CSL is around 27 m below mean sea level. Owing to its land-locked nature, the Caspian Sea level (CSL) has fluctuated repeatedly over the last millennia. This led to significant changes in its size, especially in the north where a large part of the Volga delta is now emerged.

Springer

The rationale for this study is the considerable impact (1) of rapid water level changes on the economy of the coastal area and (2) of climatic change on the region with likely further teleconnections. Large cities such as Baku are expanding right on the edge of the Caspian Sea and must integrate in their development plans the variability of the CSL. Kalmikia, the northern Caspian Depression, suffers from one of the most extensive desertification vulnerability of Europe (UNEP-Dewa, 2003). The high precipitations in the SW shores of the CS give rise to intensive agricultural activities in an otherwise dry region (Molavi-Arabshahi et al. 2015). It is thus essential to obtain correct estimations of future CS levels. Several past investigations estimated the CSL from the water budget of the CS, e.g. Arpe et al. (2014) for the present and Kislov et al. (2012) and Renssen et al. (2007) for past events, though the latter used a model without a CS. Climate models are so far very rigid concerning the size of the CS, hence introducing errors in the water budget of the CS. No attempt has been made to correct the water budget of the CS for such changes in sizes, which is the aim of this study. Many investigations, such as Arpe et al. (2000), have tried to find forcings by the large-scale atmospheric circulation on the CSL. But only few investigations have focussed on the opposite (Marković et al. 2014), which is another goal of this study.

After introducing the model, giving some background and validations of the simulations, we explain possible feedbacks. Based on the robustness of the results, a formula for a correction is provided.

Finally, impacts of the size of the CS on the general atmospheric circulation are shown with a validation using observational data.

2 Caspian Sea setting

The CS is a large endorheic water body made up of three basins, deepening from the very shallow north (5–10 m deep) to the deepest south (maximal water depth 1025 m). The middle basin has a maximum depth of 788 m.

Because of its great meridional extension, the CS straddles several climatic zones. The northern part of the drainage basin lies in a zone of temperate continental climate with the Volga catchment well into the humid mid-latitudes. The emerged Volga delta (the Caspian Depression) consists in lowlands and is very dry. The western coast features a moderately warm and dry climate, while the southwestern and the southern regions fall into a subtropical humid climatic zone. The eastern coast is desert.

The CSL has changed widely and often dramatically in the past: during its geological lifetime by more than 150 m, possibly several hundreds of meters (Forte and Cowgill 2013), during the Holocene by several tens of meters (Kakroodi et al. 2012), during the last millennium by c. 10 m (Naderi Beni et al. 2013) and during the last century by > 3 m (Arpe and Leroy 2007). In the High Medieval period (AD 1000–1300), Naderi Beni et al. (2013) have shown a clear rise of the CSL partially caused by climate and partially by humans, from 33 to 25 to 19 m bsl. Because of this and of the economical context, we choose to focus our experiments with heights up to 6 m lower than the current CSL and up to 12 m higher than the current level.

3 Material and methods

The CS grids for various water levels are determined using the ETOPO1 data set that has a horizontal resolution of 1 arc minute (Amante and Eakins 2009). If the water level of a grid point is higher than the mean bathymetry of the grid, the grid is set to be an ocean grid (Table 1).

The actual size of the CS according to the definition using this data set and method 428,500 km^2) at − 27 m is considerably larger than the generally referred size of 371,000 km^2 (e.g. Arpe et al. 2000 or https://en.wikipedia.org/wiki/Caspian_Sea) for the present CS; possibly the latter value comes from investigations that included the period of the 1970s, a time when the CSL was much lower than presently.

The ECHAM 5.4 (e.g. Hagemann et al. 2006; Roeckner et al., 2006) atmospheric model is coupled with the Taiwan Multi-scale Community Ocean Model (TIMCOM) (Tseng and Chien 2011; Young et al. 2012) in this study to quantify the impact of the CS size on the water budget of the CS and the resulting water level change. The coupled model is denoted as European Hamburg Taiwan (EHTW) model. The current

Table 1 Experiments, their CSL and CS size. The names of the simulations refer to the CSL, i.e. H27 to a CSL of − 27 m

Experiments	CSL	Actual CS size in km^2	CS size in km^2 with a T63 grids	Number of grids
H33	− 33 m	288,400	228,700	7
H30	− 30 m	331,800	260,900	8
H27	− 27 m	428,500	321,200	10
H19	− 19 m	518,500	439,900	14
H15	− 15 m	567,000	469,100	15

version of TIMCOM is advanced from the Dietrich Center for Air Sea Technology (DieCAST) model (e.g. Dietrich, 1998; Tseng et al. 2005). It solves the three-dimensional primitive equations for fluid motions under the hydrostatic and Boussinesq approximations. It uses a Z-level stretched vertical coordinate and a blend of collocated and staggered horizontal grids based on spherical coordinates with non-uniform latitudinal increments. The free-surface version of TIMCOM is applied here (Young et al. 2012). The calculation is carried out with the standard nonlinear equation of state for the in situ density in terms of potential temperature, salinity and pressure depth. Weakly physical-based parameterization is applied for the horizontal mixing (Smagorinsky 1963). The temporal discretization is based on a modified leap-frog scheme (Young et al. 2014) and the spatial discretization employs the fourth-order-accurate spatial discretization. An efficient and accurate biconjugate gradient stabilized method (BiCG solver) (Van der Vorst 1992) is used for solving elliptic partial differential equation for pressure, which is also ideal for parallel computing. See Tseng et al. (2012; 2017) and Young et al. (2012) for more model details. The ocean model is applied only for the CS, as the SST and sea ice data over the oceans and other surface parameters are taken from a 1000-year simulation (Jungclaus et al., 2010).

The major model advance in the EHTW coupled model is its inclusion of a Snow/Ice/Thermocline (SIT) solver in between the atmosphere and ocean models, which solves the vertical heat diffusion equation for temperatures in snow, ice and water column in a tri-diagonal matrix (Tsuang et al. 2001). The solver has recently been improved for ocean cool skin simulation (Tu and Tsuang 2005), better SST formulation (Tsuang et al. 2009; Lan et al. 2010) and Madden-Julian Oscillation simulation (Tseng et al., 2015; Chang et al. 2015). This solver is unconditionally stable. Since the melting and refreeze of a thin sea ice, as well as the warm layer and the

cool skin in the upper few meters of a water column can be resolved in SIT, it provides a unique surface diurnal cycle of the ocean within the climate models. Only a few climate models have explored the importance of such a diurnal cycle (Large and Caron, 2015).

A north–south profile at 51 °E of the summer SST is created by the model and by satellite observations (http://polar.ncep.noaa.gov/sst/ophi) (Fig. 1). The model produced SSTs for the beginning of the High Medieval period boundary conditions (AD 1050–1100), while the observation is for the present (AD 2001–2013). Because the CS SST increased by 2 °C during the last 30 years (e.g. Arpe et al. 2014), the observations by satellite are around 3 °C warmer than the High Medieval model simulations.

The model was running with a T63 resolution and therefore it does not have the NE bay of the CS as ocean, nor the Kara-Bogaz Gol. The topography when smoothing with a T63 resolution gives heights of + 170, − 200 and − 120 m from south to north over the sea, when it should be close to − 27 m (Fig. 2). This implies some smoothing in the orography and the shape of the CS, which is known as a Gibbs phenomenon. Figure 2 shows the CS and its surrounding orography using a 0.5° grid (right) and with a T63 (left) resolution. The Gibbs phenomenon is not as clearly indicated in Fig. 2 as by grid point values themselves; because the contouring package does not resolve nearly singular values. A heavy line shows the sizes of the CS in a T63 resolution for a CSL at − 27 m. In Fig. 3, similar heavy lines show the size of the CS at − 15 and 19 m (left) and − 33 m (right), two possible values in the last millennia. Because of the high Caucasus Mountains, the smoothing, needed for a T63 resolution, increases the topography for the middle CS basin to higher than 100 m, reaching 200 m along the western and eastern coasts (Gibbs phenomenon). The ocean model for H27 has a surface at − 27 m everywhere while the lowest atmospheric model level deviates
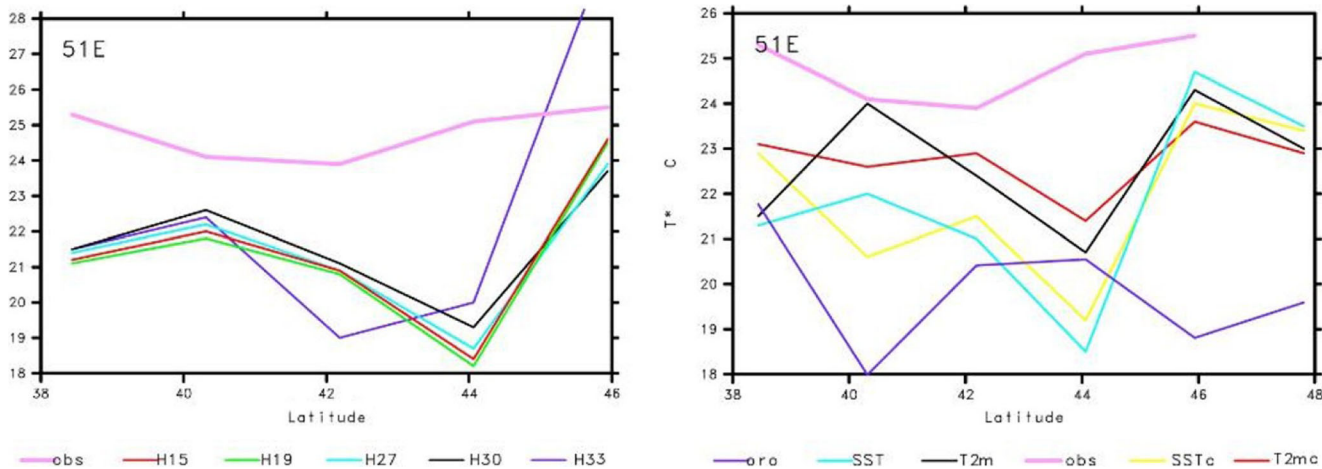

Fig. 1 Summer (June–July–August) SST of the CS along 51° E as simulated with medieval time boundary conditions (AD 1050–1100) for different CS sizes and as observed (by satellite). Left, uncorrected for all simulations; right, applying a correction of 0.8 °C/100 m for the H15 experiment (SSTc, T2mc)
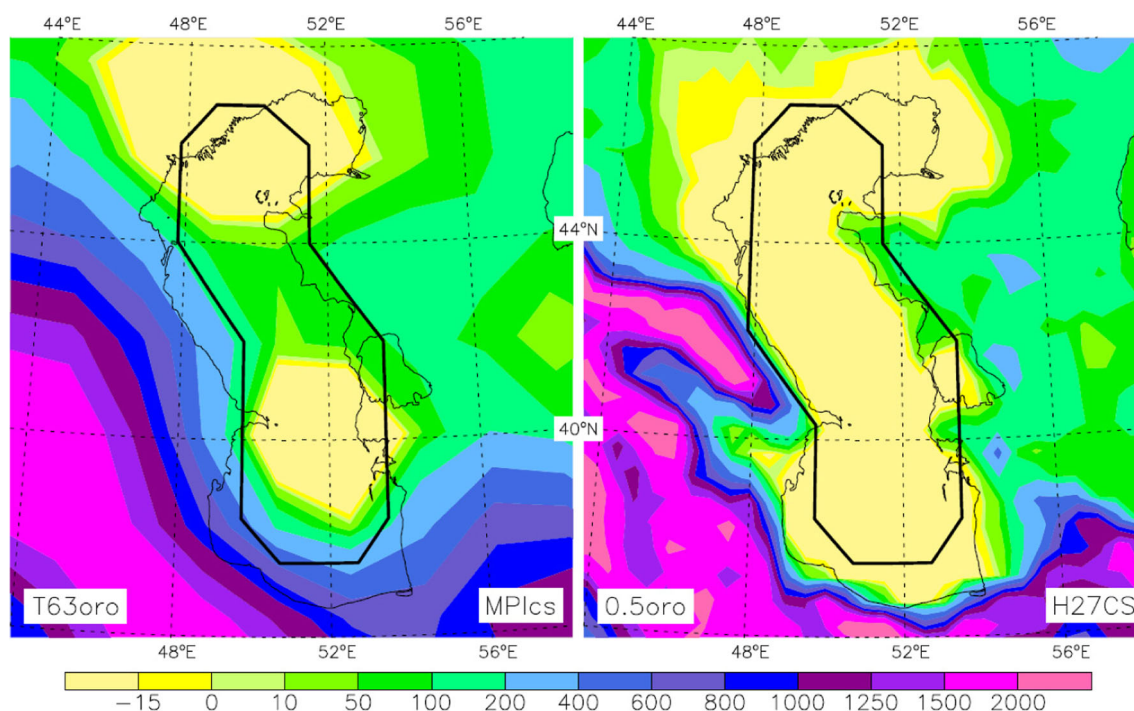
Fig. 2 Orography around the CS using a resolution of T63 (left) and 0.5° (right). Heavy line, size of the CS on a T63 grid for the CSL of − 27 m as used by MPI as a standard

from this by up to 200 m in the middle CS basin, which can lead to temperature differences as shown in Fig. 1.

A mean atmospheric temperature lapse rate of 0.8 °C per 100 m between the lowest level of the atmosphere and the − 27-m level of the CS of about − 1.3, + 1.6 and + 1.2 °C results from these differences. The SST and T2m are high when the orography is low and vice versa, i.e. T2m is low on top of a mountain and high in the valley. The atmospheric model knows only the topography on a T63 grid. Applying such a correction gives the N-S profiles in Fig. 1 (right) for the H15 simulation. A much better similarity between observation and simulation is achieved when taking the bias due to the Gibbs phenomenon

into account. Important for the discussion below are the relatively high temperatures in the northern CS (because very shallow) and in the south (because of the lower latitude).

The observations have warm temperatures at the most southern grid point (subtropical climate) while the uncorrected simulations have warmest temperatures one grid point further north due to the topographic waves over the sea generated by the Gibbs phenomenon (Fig. 2). Below, we will investigate only differences between different simulations and as all simulations suffer from the same biases (Gibbs phenomenon), we assume that our results will be less affected.

Fig. 3 Annual mean precipitation; units, mm/month. Left, in the H15 simulation. Heavy line, size of the CS on a T63 grid for the CSL of − 19 m (H19) and − 15 m (H15), the latter is one grid point larger. Right, precipitation in the ERA analysis and as a heavy line the size of the CS at − 33 m (H33)
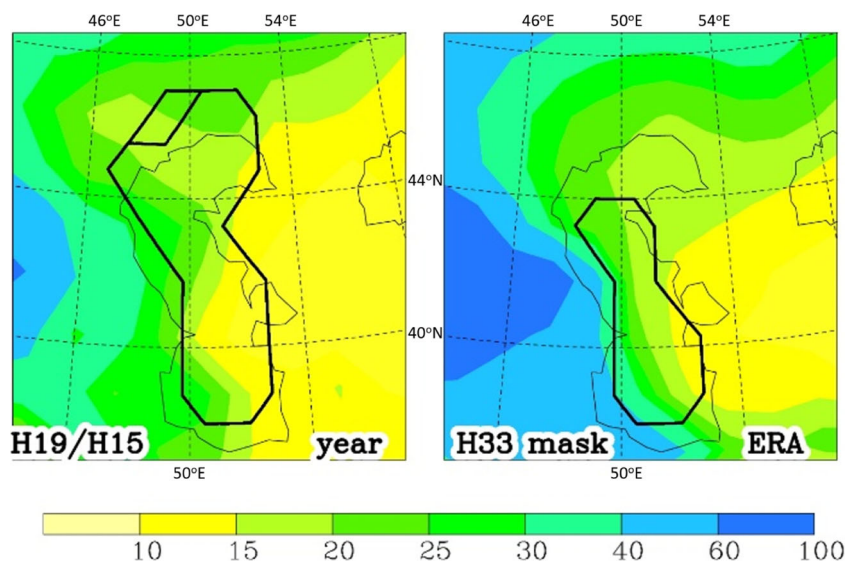
4 Model precipitation, temperature and winds

The annual mean precipitation as simulated with the H15 is compared to annual mean precipitation as estimated by the ECMWF interim re-analysis (ERA-Dee et al., 2011) (Fig. 3). The patterns in the simulation look realistic, although with too low precipitation amounts in the simulation over the Caucasus Mountains probably due to a too smooth topography (Fig. 2). The comparison with ERA is not completely justified as the ERA data are for the present and the model simulations for the low stand at the beginning of the High Medieval period but both show similar distribution features.

The annual mean wind over the CS is blowing mostly from the northeast near the surface (Fig. 4 lower panels) and from the west at 700 hPa or higher levels (Fig. 4 top panels). Such a counterflow between the two levels can be explained as a wake in the generally westerly flow disturbed by the Caucasus Mountains. The surface wind from the dry eastern plains is blowing over the CS towards the mountains in the SW of the CS and picks up moisture over the sea. In the SW of the CS, the wind path is blocked by the mountains and by the westerlies at higher levels that are descending down the mountains. This leads to an uplift of the air leading to intense precipitation especially along the NW coast of Iran, in the area of the towns of Anzali and Rasht (see Fig. 4 in Leroy et al. 2011; Molavi-Arabshahi et al. 2015).

There the convergence of the wind near the surface occurs in the analysis (ERA). It is strongest in the plains between the mountains and the coast where the heaviest precipitation is observed. It is to be seen more over the sea in the model simulation due to the smoothing effect when using a lower resolution that leads to a downward slope of the mountains reaching into to the CS. At this convergence (Fig. 4), we expect the strongest precipitation changes when reducing the size of the CS. The enhanced precipitation in the SW of the CS can be seen in Fig. 3 for ERA while it does not stick out for the model simulation.

5 Interactions between evaporation and precipitation

When the CSL falls, the size of the CS is shrinking. As the ocean area is the main source of water to the atmosphere via evaporation, less water will be available in the atmosphere when the CS is small. Less water in the atmosphere should decrease the precipitation in the surrounding of the CS and over the CS itself. With falling levels, the CS becomes smaller and so less evaporation occurs, which reduces the drop of the

Fig. 4 Annual mean wind field at 700 hPa (top panels) and 10 m (lower panels) as analysed by ERAinterim (right) and simulated by the H27 model (left). Arrows show the wind direction with the length proportional to wind speed. Contours, wind speed calculated from the averages of wind components
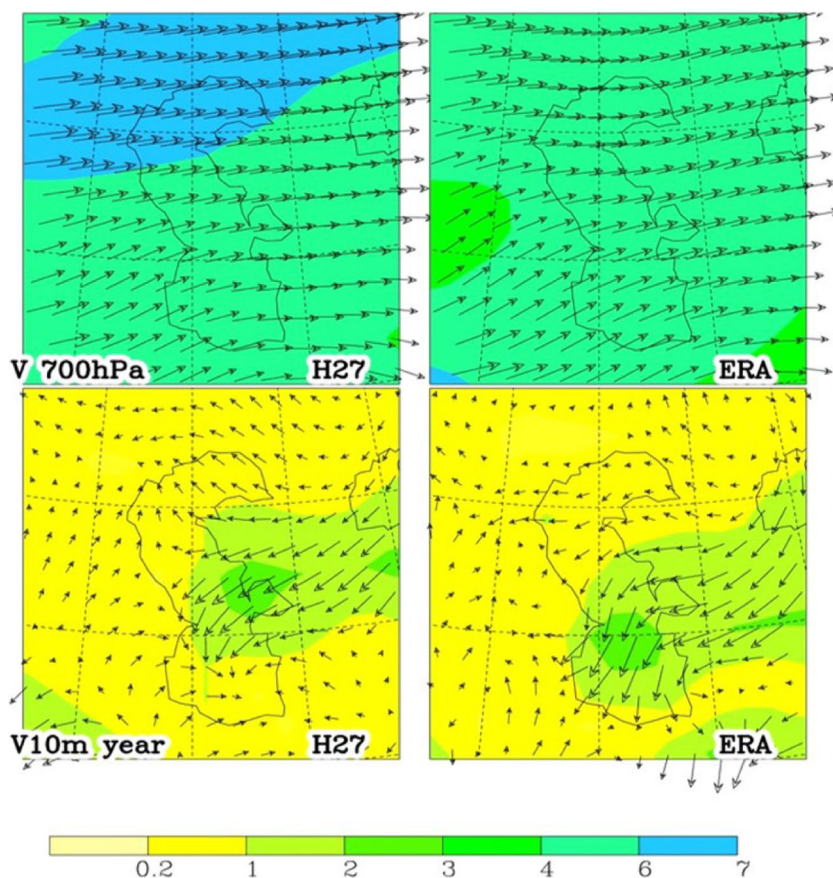
CSL (negative feedback—A). With less water in the atmosphere, the precipitation over and around the CS will be reduced leading to an enhancement of the drop of the CSL (positive feedback—B). With less precipitation over the continent, less water in and on the ground is available for evaporation (a negative feedback for the fall of the CSL—C). Feedback A is likely to be the largest followed by B and then C. This sequence can of course continue for more evaporation—precipitation cycles. The simulations will show only the total effect of these combined feedbacks.

Evaporation in experiments with larger CS sizes is compared with that of smaller ones (Fig. 5). H15 is expected to have the largest evaporation amounts over the CS itself and H33 lowest, especially where the land has emerged with lower CSL and smaller CS sizes. Indeed these areas appear as bull's eyes with large positive values. The evaporation over the continent is expected to be largest where the precipitation is largest. Indeed, when comparing evaporation (Fig. 5) with precipitation (Fig. 6), a strong similarity can be found.

From the arguments given above, one expects more precipitation in the experiments with larger CS sizes, especially over the SW coast of the CS. This can be found more or less in the precipitation (Fig. 6); but larger increases of precipitation occur north of the CS, i.e. where the CS loses a large area because it is shallow. The enhanced precipitation over the northern grids in H15 and H19 might cause an atmospheric circulation upwards over these points and downwards around it, similarly as found by Tsuang et al. (2001), which might explain the reduced precipitation and evaporation at some distance northwest of the CS.

Further, the evaporation over the southern CS is larger in the experiments with a smaller CS (Fig. 5). One reason for that could be that with a smaller CS, the air flowing over the CS is dryer because of its shorter fetch over the water body when reaching the southern CS. Probably more important is the lower SST (down by as much as 1.5 °C) in the southern CS (four grid points that are ocean points for all resolutions because of the deep sea there) with a larger CS in summer, the season when the evaporation is largest (Fig. 7). For summer, a larger CS means more total evaporation for the CS, especially in the northern shallow part where the SST becomes very warm (see Fig. 1). This means an enhanced loss of energy for the total mass of water. As the mass of water of the CS hardly changes with a higher CSL (up to 18 m compared to a
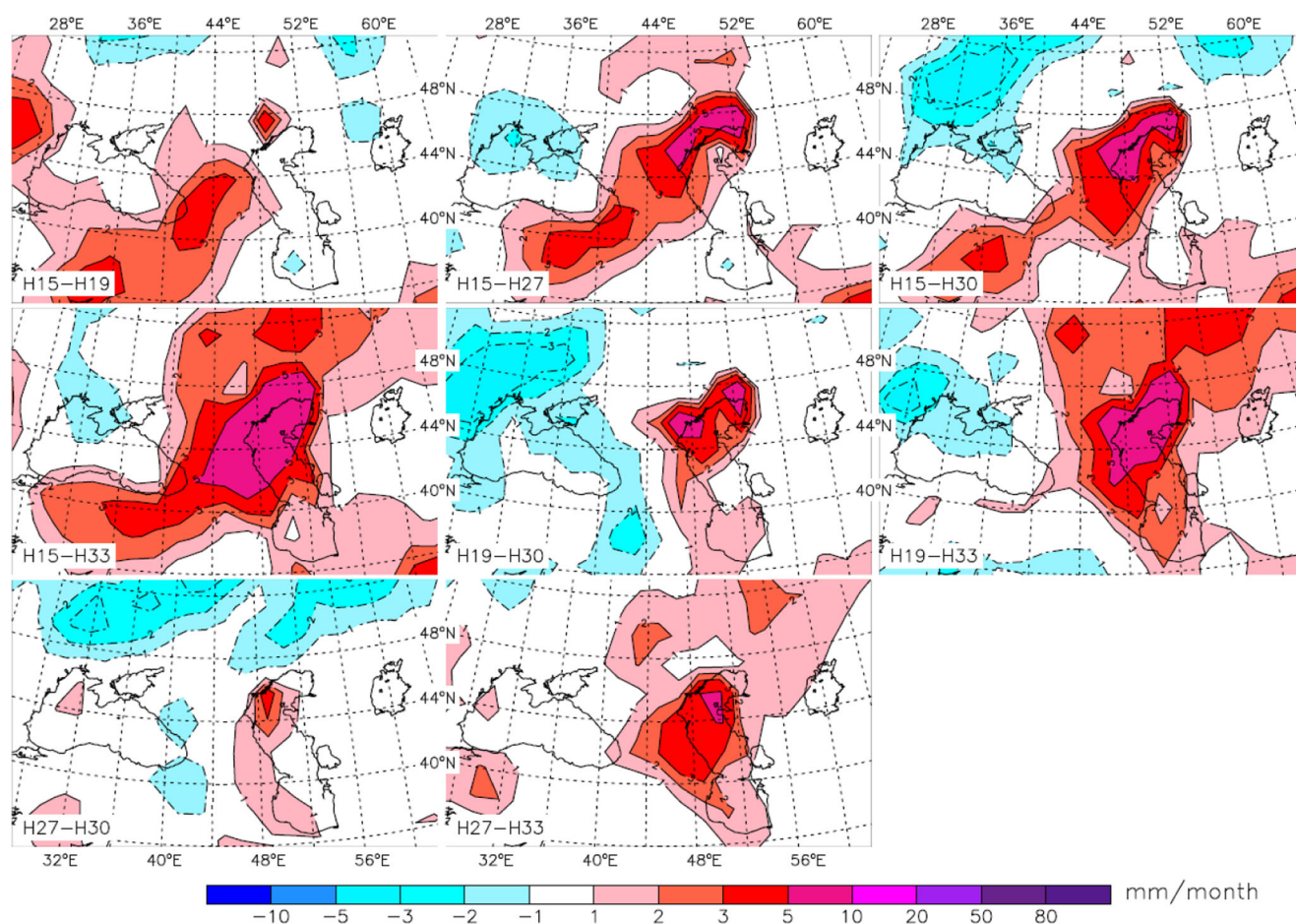

Fig. 5 Differences of annual mean evaporation in the experiments, higher CSLs minus lower CSLs
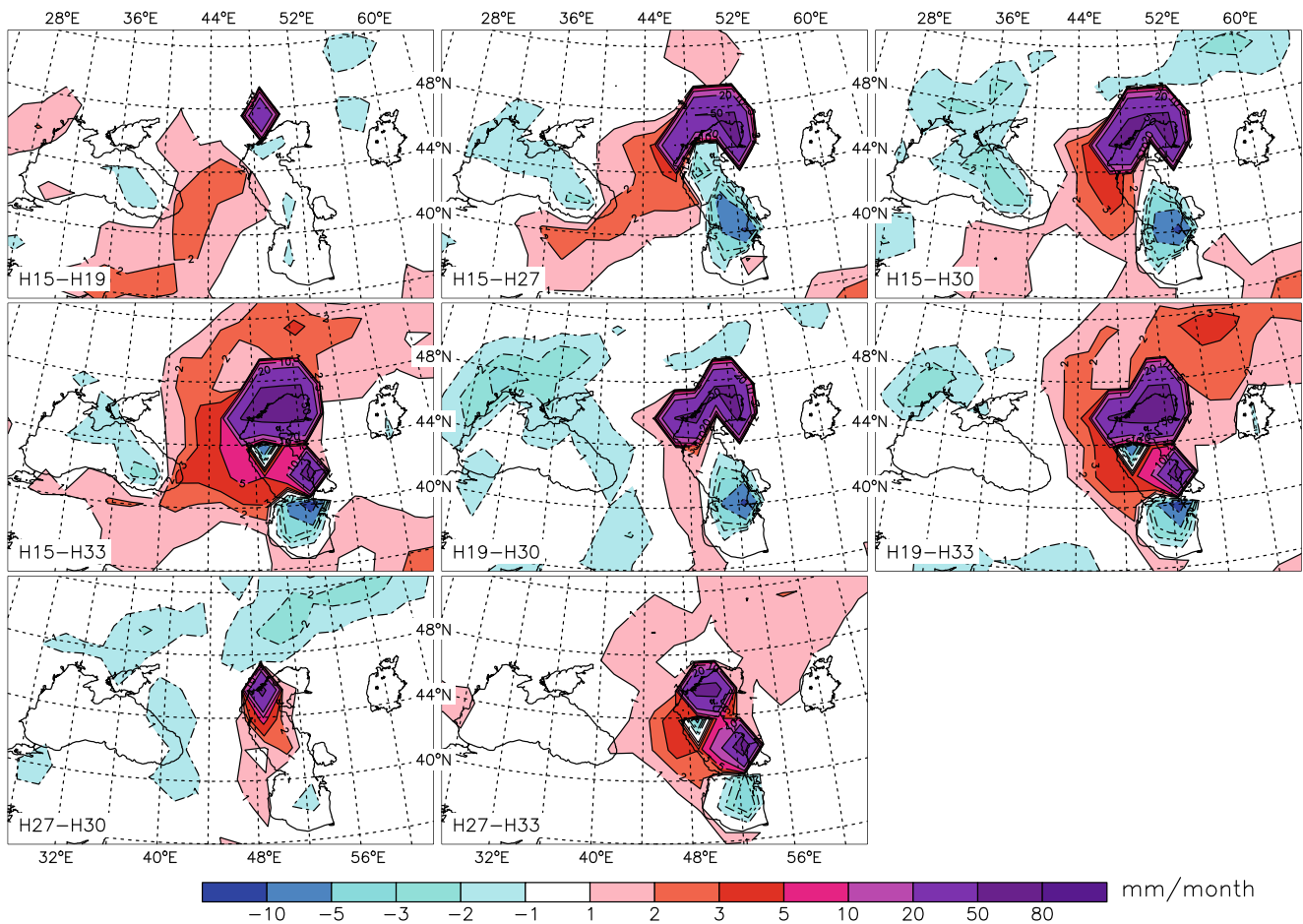
Fig. 6 The same as Fig. 5 for precipitation

mean depth of the sea of about 210 m) and as the ocean model distributes this loss of energy horizontally, this enhanced evaporation could lead in summer to a reduction of the SST also in the southern basin. The relative larger sea ice cover in the larger CS (Fig. 8), which inhibits evaporation in winter, leaves more energy in the sea leading to higher temperatures also in the southern grid points in winter for a larger CS size.
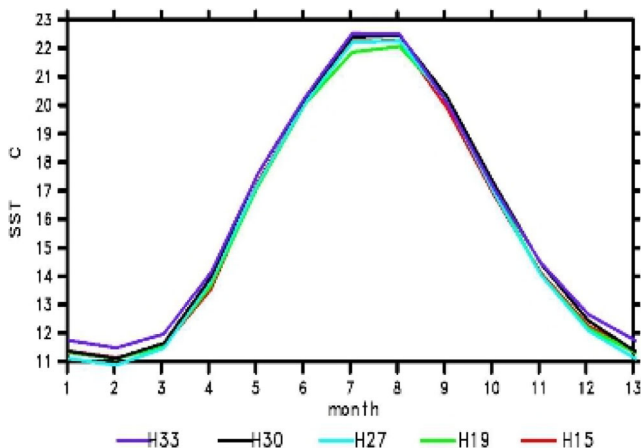

Fig. 7 Annual cycle of the SST over the southern CS (the four southern grid points in a T63 resolution) of the five experiments

In Table 2, the evaporation and precipitation for the two experiments with extreme CSLs over the CS itself (grid points of the H15 experiment), over the continent of the catchment of the CS (rivers) and precipitation–evaporation (P-E) for the whole catchment of the CS, are presented. As H15 has little more than twice the amount of grid points for the CS compared to H33, one expects H15 to have similarly more evaporation over the CS as H33. This is not completely true as the grid points which become land at a CSL of −33 m will still have some evaporation and because the SSTs especially in summer, when the evaporation is highest, the experiments with smaller sizes are warmer (meaning more evaporation) than those with larger sizes (Table 2).

The amount of evaporated and precipitated water over the CS itself involved in the experiments is however small compared to the values over land, here called rivers. The feedbacks, A, B and C, create differences of precipitation over the whole catchment between the runs, which are of the same order of magnitude as the original evaporation difference over the CS itself. The sum of differences of P-E for the whole catchment area of the CS is smaller than that of the evaporation over the CS, i.e. from 13.3 (CS) to 9.5 km^3/month, i.e. only 71% of the reduced evaporation in a smaller CS results

Fig. 8 SSTs during winter in experiments H27 and H15 in colour overlaid in solid lines the ice cover (contours at 20, 40, 60 and 80% ice cover of a grid point)
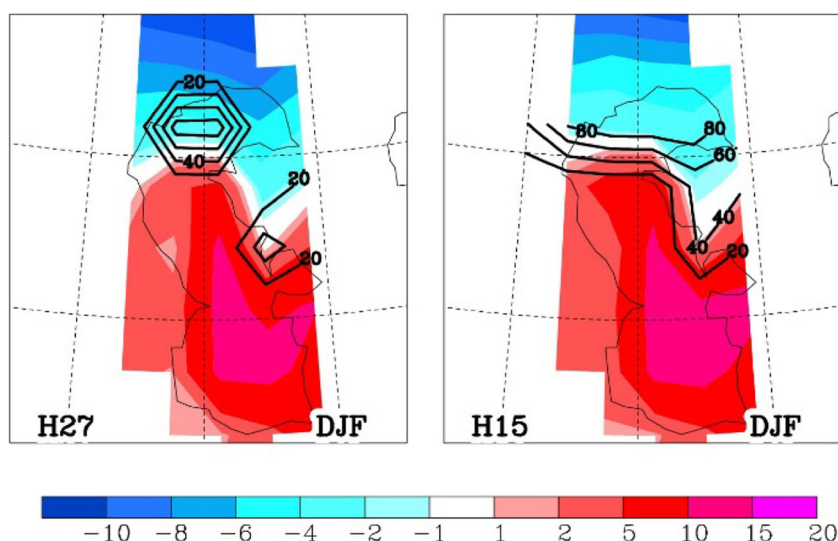
into a reduction of the water budget of the whole CS catchment area due to the feedbacks.

In a simulation with a closed water budget, the P-E values should be near zero for a closed catchment area like the CS catchment when the simulation is in equilibrium, which is obviously not the case. In present models, the oceans and lakes are unlimited sources for water and the river discharges are somehow distributed into the oceans. For comparison, the present observed Volga discharge is 20.9 km^3/month. In Table 2, P-E for all rivers is given as 25 or 28 km^3/month, i.e. the presently observed discharge is near the generally given 80% of total river discharges in the model simulations. The larger amount of water coming from the rivers than E-P over the CS itself does not compensate to gain equilibrium.

In Fig. 9, all pairs of differences of grid point versus components of the water budgets in the experiments with different CSLs are compared. As the markers are well clustered along a diagonal for the evaporation over the CS, the linear relation between the number of grid point differences and the evaporation differences appears very stable (the diagonal gives 0.68 change of evaporation pro change of grid) and so is the relation to P-E differences for the whole catchment area (the diagonal gives 0.9 change of P-E pro change of grid). The relation between the number of grid point differences and the

precipitation differences over the whole CS catchments area is the least robust one, and it is hardly justified to draw a diagonal line for that. The variability of precipitation in time is much larger than the signal from the evaporation differences over the CS.

6 A practical application: calculation of the CSL from experiments with a different CS size

The practical use of these experiments is that with a change of the size of the CS by X%, the evaporation over the CS itself will change by slightly less of that percentage and the final effect for P-E over the whole catchment of the CS is only 50% of the change of evaporation over the CS itself.

$$P-E.catch, r = P-E.catch, a-EVcs, a*(AREAr-AREAa)/AREAa*0.5 \quad (1)$$

Equation (1) is used to estimate P-E for the whole catchment area of the CS from a simulation which has a CS size different to the requested one, where a = from available experiment, r = for requested CS area and AREA = area of CS itself.

Table 2 Evaporation (Evap), precipitation (Precip) and P-E for different areas of the experiments H19 and H33, i.e. the experiments representing the two extreme CSLs, and their differences. Units, km^3/month. Some inconsistencies may have resulted from rounding

	Evap CS	Precip CS	P-E CS	Evap rivers	Precip rivers	P-E rivers	P-E all CS catchment
H15	28.9	8.6	20.3	65.8	90.4	25.4	4.2
H33	15.6	6.2	9.4	62.7	90.7	28	13.7
H15-H33	13.3	− 2.4	10.9	3.1	− 0.3	− 3.4/− 2.6	9.5

Fig. 9 Scatter diagram correlating the difference of number of grid points, representing the CS, and differences of evaporation, precipitation or P-E with different CS sizes. Squares represent cases using H15 experiments and crosses the other ones. Units, km³/month
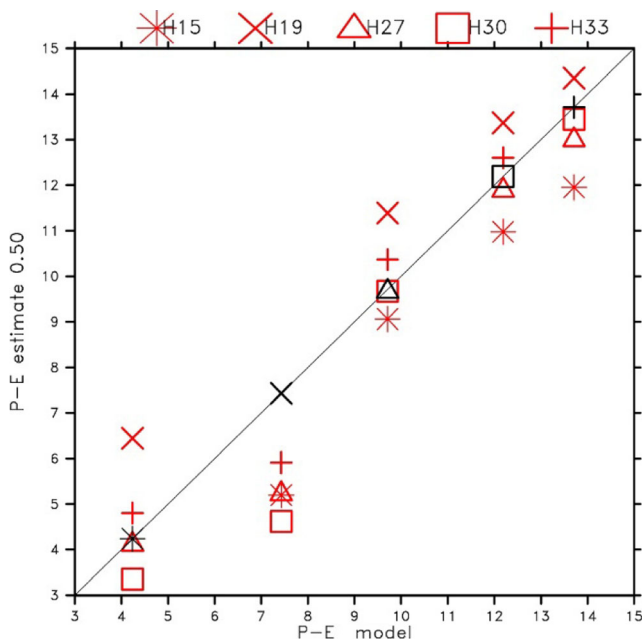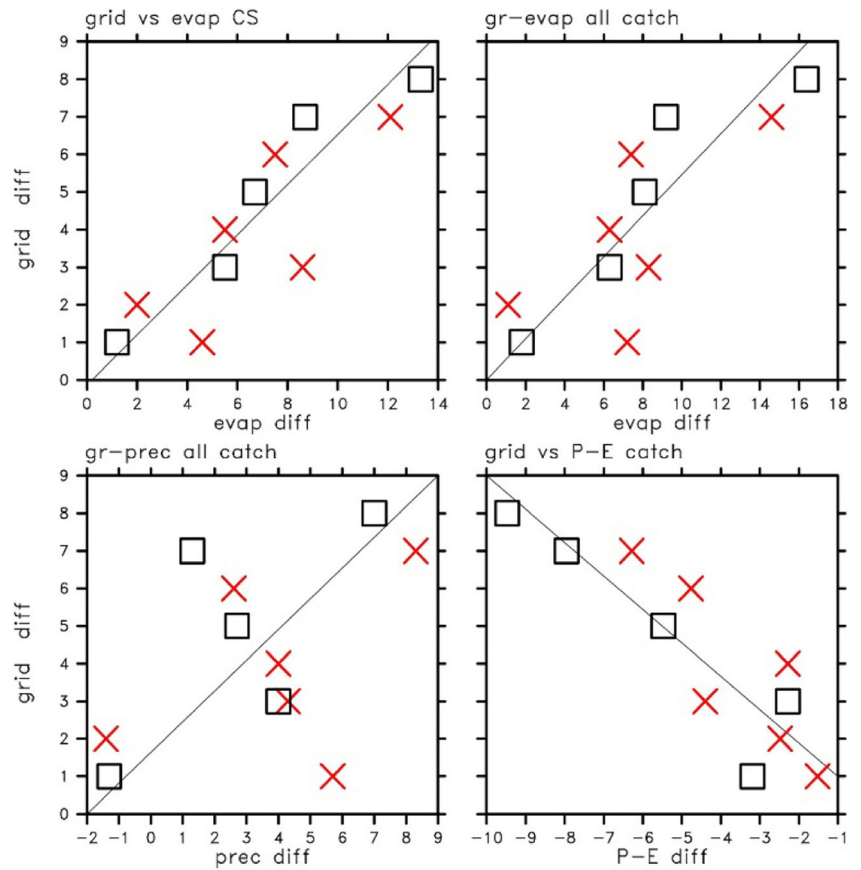
Fig. 10 Scatter diagram correlating P-E for the whole CS catchment with different CS sizes as simulated by the model and as estimated from simulations with different CS sizes, applying the method described in the text. The different markers indicate from which experiment the estimates have been made. The targets for the estimates are the black markers on the diagonal. Units, km³/month

If one wants to investigate the water budget of the CS for a simulation with a model that uses a constant CS size, say the one of the CSL at − 27 m, for a period of large variations of the CSL as during the High Medieval times, we suggest to use the evaporation over the CS itself, and multiply it with the relative CS size differences. This provides the change of evaporation over the CS itself. Due to the feedbacks, only 50% of this change has to be added or subtracted from P-E over the whole CS catchment obtained from the model simulation with constant CSL.

All P-E differences of the simulations with different CS sizes are compared with all possible estimates of P-E from simulations with different CS sizes by the method described above (Fig. 10). The experiment numbers, on which the estimates are based, are indicated by different markers and the model results, for which the estimates aimed for are indicated by black markers on the diagonal. A very good correspondence can be found. Only when the H19 experiment is involved larger deviations are found.

Originally, we planned only to carry out experiments H19 to H33. Because of the exceptional behaviour of H19, we added H15 with one grid point more than H19 to see if a threshold with increasing CS sizes may be the cause for the exceptional behaviour of H19. It is shown here that H15 fits very well with the smaller sized CSs and H19 is exceptional for other unknown reasons.

Table 3 Annual mean SST over the CS (H15 size) with different sizes of the CS in the model

	H33	H30	H27	H19	H15
SST	13.10	13.13	12.74	12.45	12.37

7 Importance of using a full ocean model for the CS

In Fig. 7, differences of the annual cycle of the SSTs over the southern CS were shown and it was speculated about those differences. Table 3 shows that, for the whole CS, the annual mean SSTs increase with decreasing CS sizes reaching a 0.63 °C difference between H15 and H33. This is a consistent signal through the 50 years of simulations.

Hand-waving arguments are that more energy loss occurs in summer, when evaporation is largest, with a larger CS size by evaporation in the very warm northern part of the CS. This results in excessive losses of energy for larger CS sizes leading to a reduction of the SST for the whole CS, because of an exchange of energy between the northern and southern CS by the ocean model (N to S exchange also seen in oceanographical and sedimentological observations; Lahijani et al. submitted). The reduced evaporation during winter with larger CS sizes due to extended ice cover that prevents evaporation in the northern part with larger CS sizes is less strong (Fig. 7), and therefore the summer effect is reflected by the annual mean. The available data are not sufficient to show if imbalances of energy between the shallow and deep parts of the CS by the ocean model are compensated and a repetition of the simulation without energy exchange between ocean grid points would give an answer.

8 An application for calculating the CSL during the Last Glacial Maximum

Several attempts have been made to estimate the CSL during the Last Glacial Maximum (LGM, c. 21,000 years ago) from water budget calculations (e.g. Kislov et al. 2012). Due to the lower temperatures, the precipitation and the evaporation over the CS basin were reduced during the LGM resulting in polar desert conditions in some parts of Europe (Crowley and North

1991; Panin and Matlakhova 2015); but the balance between both components is difficult to estimate.

Possible but unlikely diversions of northward flowing rivers to the south due to glaciers along the Arctic coast or of the Amu-Darya will be ignored here. Available to us are the experiment with a T106 ECHAM5 model used by Arpe et al. (2011) and the CMIP5 simulations provided by the Max-Planck Institute for Meteorology with a T63 ECHAM6 model (Jungclaus et al. 2010). Both simulations give initially very different values for the averaged water budgets (Table 4). The CMIP5 simulations consist of two simulations for the LGM with similar results.

As the T63 simulation has a much smaller CS (Table 2) than in reality, we corrected P-E for the whole catchment using 50% of the evaporation over the CS multiplied by the ratio of CS size differences divided by the CS size of T63 (Eq. (1)). For simplicity, only the T63 simulations were corrected to the T106 CS size, as the latter is near to the true size. The CS size for T63 in Table 3 differs from that in Table 2 because CMIP5 uses a different land-sea mask (one ocean point more on the west coast for the middle basin; Fig. 2) than that used in this study. Atmospheric models are not perfect yet and one has to assume that they suffer from systematic errors. To reduce their impact, we investigate the changes between the present and the LGM, which result into very similar water deficits for the LGM, i.e. the CS must have been smaller in order to gain a balanced water budget. For calculating the CS size during the LGM from the water deficit, one can use the same formula (Eq. (1)) used above but resolving it for CS size difference between the present and the LGM. The results are:

For T63 ECHAM6: 303,666 km^2 or 79% of the present, which corresponds to a CSL of −30 m

For T106 ECHAM5: 286,945 km^2 or 74% of the present, which corresponds to a CSL of −33 m

Although we started with different numbers from the two different sets of simulations, both came to similar CSLs for the LGM, i.e. lower than now by several meters.

The level of the CS in the LGM is not well known and differs widely between various geological investigations. The levels may have been much lower than those at present and may correspond to the Atelian or Enotayevian lowstand that reached perhaps 50 to 150 m bsl (Chepalyga 2007; Svitoch 2009; Tudryn et al. 2013).

Table 4 Water budget values for the present (CTR) and the Last Glacial Maximum (LGM) with two experiments. Units, km^3/month

	CS size CTR km^2	Evap CS CTR	P-E all catchment CTR	Corrected for size of T106	P-E all catchment LGM	Water deficit for LGM
T63 ECHAM6	352,700	−337	7.8	22	60	38
T106 ECHAM5	382,658	−304	75		111	36

Mamedov (1997) suggests a much lower CSL of − 50 m from several strands of evidence, such as by the erosion of knolls, the occurrence of a 20-m high cliff separating Early and Late Khvalynian terraces on the Mangyshlak peninsula and the deep incision of the Volga and the Uzboi. Climate modelling for the LGM (Arpe et al. 2011) suggests a lower level than that today.

To the contrary of this, water levels higher than those at present have also been proposed. A water level of 15 m bsl is suggested by Klige (1990) and 25 m asl by Toropov and Morozova (2010). Tudryn et al. (2016) suggest including the LGM in the first part of the early Khvalynian transgression.

9 Impact of the CS on the large-scale circulation

For winter, a larger difference of the 500 hPa height field between H19 and the other experiments can be found over the northern Pacific (Fig. 11). The differences between the experiments are small compared to the horizontal variations; so that differences can hardly be seen (Fig. 11 upper left panel). But the difference maps between H15 or H19 and the other experiments in the other panels show a very consistent signal of up to 40 geopotential m for H33-H15 around 160° W and 50° N which means that the Aleutian
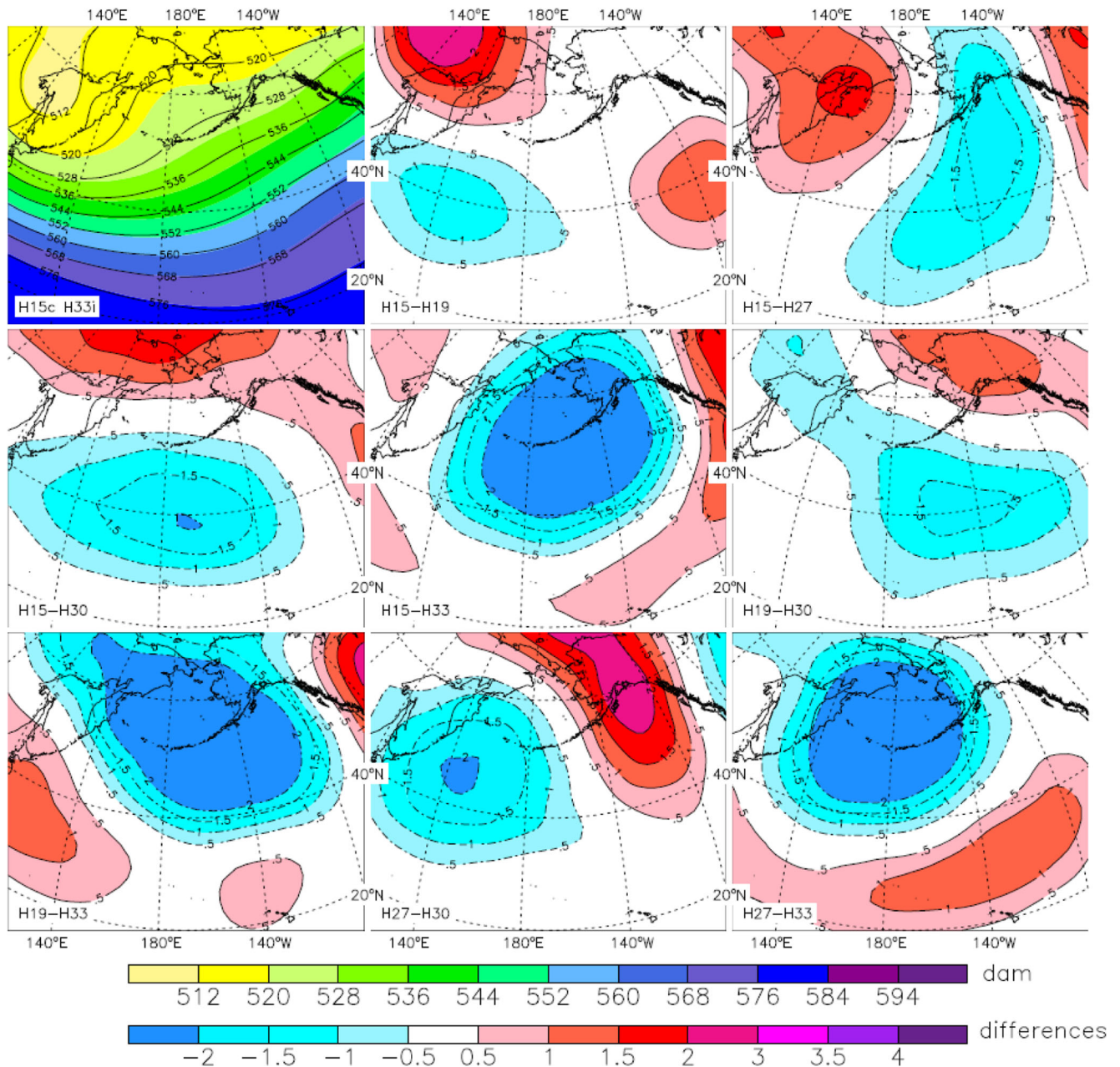

Fig. 11 DJF mean 500-hPa height field. Units, geopotential decameters. The upper left panel shows the contours of H15 in colours and of H33 as lines. The other panels show the differences between H15, H19 or H27 and the experiments with lower CSL. Units, geopotential decameters (dam)

Fig. 12 Time series of DJF mean 500-hPa height field in the northern Pacific (160–180° W/ 40–50° N). A 9-year running mean has been used for smoothing
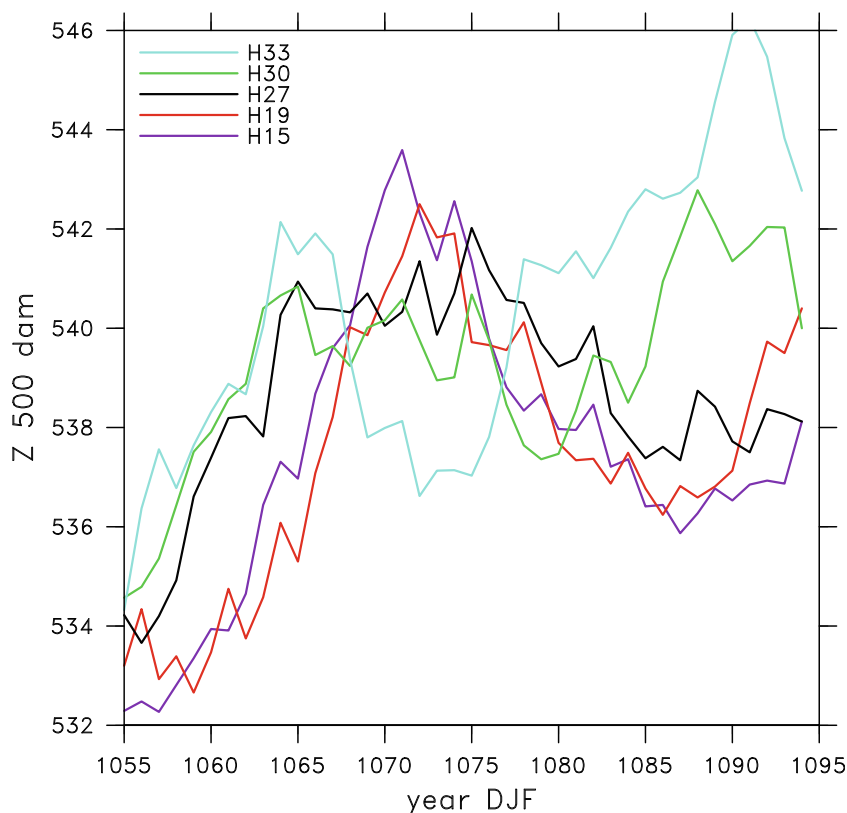
trough is expending further to the east in the experiments with a higher CSL (larger CS) or the ridge east of the Aleutian trough is weakened.

This finding suggests that the CS has a systematic impact on the large-scale circulation and with a stronger impact with a larger CS. Figure 12 shows the robustness of this impact in time
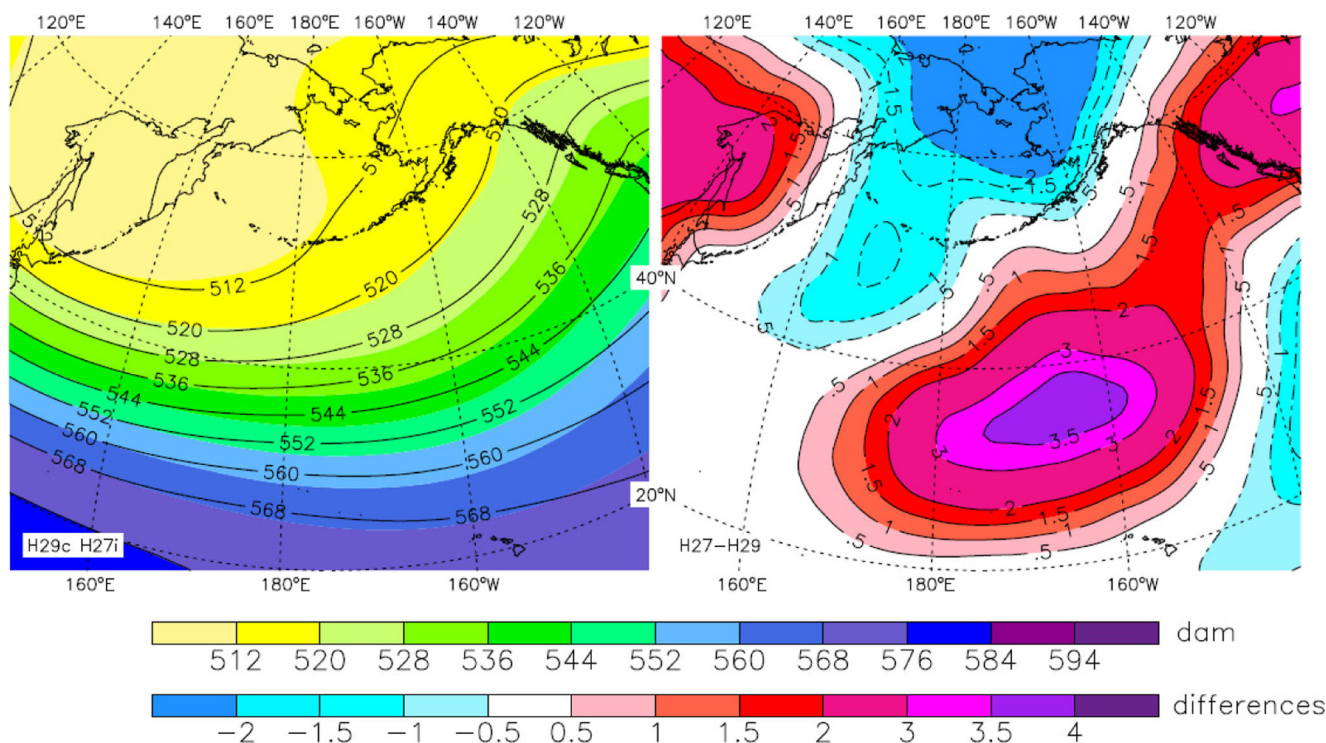

Fig. 13 The same as Fig. 11 for ERA observations for 2 periods (1979–1983 and 1992–1995) with 2-m CSL differences. Left panel, height fields in colour of period (1979–1983) with low CSL and as black lines period (1992–1995) with high CSL. Right panel, their differences

series of an area mean of the 500 hPa height field in all experiments. Although a large variability occurs in time throughout the later eleventh century, generally highest values in the H33 and H30 and lowest values in the H15 and H19 (except for a 10-year period), and it can be assumed we can assume that this robustness would be true as well for the present.

The results shown here are valid for the present model and background data and investigate possible restrictions we tried some validation with observational data.

Since 1979, ERA interim analyses (Dee et al. 2011 and ECMWF 2015) are available and one can see if the changes in the CSL during that period show an impact similar to that found here with a model. During the last 30 years, the CSL has changed by more than 2 m, lowest around 1977 and highest around 1994 (Arpe et al. 2011).

The 500-hPa height field differences of the analyses for the periods 1979 to 1983 with CSLs near − 29 m and 1992 to 1995 with CSLs near − 27 m (Fig. 13) show patterns very similar to the ones in Fig. 11. This similarity suggests that the model results are representative also of the real atmosphere.

10 Conclusions

It has been shown that the CS size is linearly related to the changes of evaporation over the sea and P-E for the whole CS catchment area, which allows an estimate of the change of the CSL from the change of the CS size when a simulation was carried out with a wrong CS size. In fact, a T63 resolution model is using a too small CS; thus, the evaporation over the ocean in such a simulation should be corrected for the size difference. The proposed formula to do such a correction turned out to be very robust.

The evaporation over the CS itself changes less strongly than one would expect from the change of numbers of grid points. A main reason is an increase of the SST over the CS with a decreasing CS size together with a larger annual cycle of the CS SST also in the southern (deep) basin of the CS with decreasing CS sizes.

Feedbacks between evaporation and precipitation suggest a large recycling of water in the catchment area of the CS. A change of evaporation over the CS itself leads to only 70% of change of the water budget of the whole CS catchment area.

The experiments showed also a clear impact of the CS on the large-scale atmospheric circulation over the northern Pacific. The larger the CS, the wider is the Aleutian trough at 500 hPa. The patterns in Fig. 11 remind of the Pacific–North American teleconnection (PNA) patterns. The PNA is connected with a wave train from the Indian Ocean via the northern Pacific and North America to the Atlantic, with largest amplitudes over the Pacific and North America. A small tickling of this wave train near its source may have a larger impact further downstream, which seems to be the case here.

Despite the good validation of our model for the impact of the CS size on the general circulation, the question remains if the results shown are only valid for the model applied here or if they are also true more generally. This can be done by repeating at least some of the simulations with a different model. More studies is needed. We have chosen to use a resolution of T63, which is the lowest resolution which represents the shape and size of the CS and with which the experiments could be carried out with the resources available to us.

References

Amante C, Eakins BW (2009) ETOPO1 1 Arc-minute global relief model: procedures, data sources and analysis. NOAA Technical Memorandum NESDIS NGDC-24. National Geophysical Data Center, NOAA. doi:https://doi.org/10.7289/V5C8276M. https://www.ngdc.noaa.gov/mgg/global/global.html

Arpe, K., & Leroy, S. A. (2007). The Caspian Sea Level forced by the atmospheric circulation, as observed and modelled. Quat Int 173: 144–152

Arpe K, Bengtsson L, Golitsyn GS, Mokhov II, Semenov VA, Sporyshev PV (2000) Connection between Caspian Sea level variability and ENSO. Geophys Res Lett 27(17):2693–2696

Arpe K, Leroy SAG, Mikolajewicz U (2011) A comparison of climate simulations for the last glacial maximum with three different versions of the ECHAM model and implications for summer-green tree refugia. Clim Past 7:1–24. https://doi.org/10.5194/cp-7-1

Arpe K, Leroy SAG, Mikolajewicz U (2014) A comparison of climate simulations for the last glacial maximum with three different versions of the ECHAM model and implications for summer-green tree refugia. Clim Past 7:1–242011, Theor Appl Climatol. https://doi.org/10.1007/s00704-013-0937-6

Chang CWJ, Tseng WL, Hsu HH, Keenlyside N, Tsuang BJ (2015) The Madden-Julian oscillation in a warmer world. Geophys Res Lett 42(14):6034–6042

Dee DP, Uppala SM, Simmons AJ, Berrisford P, Poli P, Kobayashi S, Andrae U, Balmaseda MA, Balsamo G, Bauer P, Bechtold P, Beljaars ACM, van de Berg L, Bidlot J, Bormann N, Delsol C, Dragani R, Fuentes M, Geer AJ, Haimberger L, Healy SB, Hersbach H, Hólm EV, Isaksen L, Kållberg P, Köhler M, Matricardi M, McNally AP, Monge-Sanz BM, Morcrette J-J, Park B-K, Peubey C, de Rosnay P, Tavolato C, Thépaut J-N, Vitart F (2011) The ERA -interim reanalysis: configuration and performance of the data assimilation system. Q J R Meteorol Soc 137, 656:553–597, Part A. https://doi.org/10.1002/qj828

Dietrich DE (1998) Application of a modified Arakawa 'a'grid ocean model having reduced numerical dispersion to the Gulf of Mexico circulation. Dyn Atmos Oceans 27(1):201–217

ECMWF (2015) http://apps.ecmwf.int/datasets. Last access May 2015

Forte AM, Cowgill E (2013) Late Cenozoic base-level variations of the Caspian Sea: a review of its history and proposed driving mechanisms. Paleogeogr Palaeoclimatol Palaeoecol 386:392–407

Hagemann S, Arpe K, Roeckner E (2006) Evaluation of the hydrological cycle in the ECHAM5 model. J Clim 19:3810–3827. https://doi.org/10.1175/JCLI3831.1

Jungclaus JH, Lorenz SJ, Timmreck C, Reick CH, Brovkin V, Six K, Segschneider J, Giorgetta MA, Crowley TJ, Pongratz J, Krivova NA, Vieira LE, Solanki SK, Klocke D, Botzet M, Esch M, Gayler V, Haak H, Raddatz TJ, Roeckner E, Schnur R, Widmann H, Claussen M, Stevens B, Marotzke J (2010) Climate and carbon-cycle variability over the last millennium. Clim Past 6:723–737. https://doi.org/10.5194/cp-6-723-2010

Kakroodi AA, Kroonenberg SB, Hoogendoorn RM, Mohammadkhani H, Yamani M, Ghassemi MR, Lahijani HAK (2012) Rapid Holocene sea-level changes along the Iranian Caspian coast. Quat Int 263:93–103

Kislov A, Panin A, Toropov P (2012) Palaeostages of the Caspian Sea as a set of regional benchmark tests for the evaluation of climate model simulations. Clim Past Discuss 8:5053–5081. www.clim-past-discuss.net/8/5053/2012/. https://doi.org/10.5194/cpd-8-5053-2012

Klige RK (1990) Historical changes of the regional and global hydrological cycles. GeoJournal 20(2):129–136

Lan YY, Tsuang BJ, Tu CY, Wu TY, Chen YL, Hsieh CI (2010) Observation and simulation of meteorology and surface energy components over the South China Sea in summers of 2004 and 2006. Terr Atmos Ocean Sci 21(2):325–342

Large WG, Caron J (2015) Diurnal cycling of sea surface temperature, salinity, and current in the CESM coupled climate model. J Geophys Res Oceans 120:3711–3729. https://doi.org/10.1002/2014JC010691

Leroy SAG, Lahijani HAK, Djamali M, Naqinezhad A, Moghadam MV, Arpe K, Shah-Hosseini M, Hosseindoust M, Miller CS, Tavakoli V, Habibi P, Naderi Beni M (2011) Late Little Ice Age palaeoenvironmental records from the Anzali and Amirkola lagoons (South Caspian Sea): vegetation and sea level changes. Palaeogeogr Palaeoclimatol Palaeoecol 302:415–434

Mamedov AV (1997) The late Pleistocene-Holocene history of Caspian Sea. Quat Int 41/42:161–166

Marković SB, Ruman A, Gavrilov MB, Stevens T, Zorn M, Komac B, Perko D (2014) Modelling of the Aral and Caspian seas drying out influence to climate and environmental changes. Acta Geogr Slov 54(1):143–161

Molavi-Arabshahi M, Arpe K, Leroy SAG (2015) Precipitation and temperature of the Southwest Caspian Sea region during the last 55 years: their trends and teleconnections with large-scale atmospheric phenomena. Int J Climatol. https://doi.org/10.1002/joc4483

Naderi Beni A, Lahijani H, Mousavi Harami R, Arpe K, Leroy SAG, Marriner N, Berberian M, Andrieu-Ponel V, Djamali M, Mahboubi A, Reimer PJ (2013) Caspian Sea-level changes during the last millennium: historical and geological evidence from the south Caspian Sea. Clim Past 9:1645–1665. www.clim-past.net/9/1645/2013. https://doi.org/10.5194/cp-9-1645-2013

Panin A, Matlakhova E (2015) Fluvial chronology in the East European Plain over the last 20 ka and its palaeohydrological implications. Catena 130:46–61

Renssen H, Longhead BC, Aerts JCJH, de Moel H, Ward PJ, Kwadijk JCJ (2007) Simulating long-term Caspian Sea level changes; The impact of Holocene and future climate conditions. Earth Planet Sci Lett 261:685–693

Roeckner E, Brokopf R, Esch M, Giorgetta M, Hagemann S, Kornblueh L, Manzini E, Schlese U, Schulzweida U (2006) Sensitivity of simulated climate to horizontal and vertical resolution in the ECHAM5 atmosphere model. J Clim 19(16):3771–3791

Smagorinsky J (1963) General circulation experiments with the primitive equations, I The basic experiment. Mon Weather Rev 91:99–164

Svitoch AA (2009) Khvalynian transgression of the Caspian Sea was not a result of water overflow from the Siberian proglacial lakes, nor a prototype of the Noachian flood. Quat Int 197:115–125

Toropov PA, Morozova PA (2010) Evaluation of Caspian Sea level at late Pleistocene period (on the base of numerical simulation adjusted for Scandinavian glacier melting) 134–138 Proceedings of the international conference THE CASPIAN REGION: ENVIRONMENTAL CONSEQUENCES OF THE CLIMATE CHANGE. Moscow State University, faculty of geography, Russian Foundation for basic research, 14–16 Oct., 2010. https://istina.msu.ru/collections/1550121/ http://www.ngdc.noaa.gov/mgg/global/global.html/https://doi.org/10.1002/2014JC010691https

Tseng YH, Chien MH (2011) Parallel Domain-decomposed Taiwan Multi-scale Community Ocean Model (PD-TIMCOM). Comput Fluids 45(1):77–83

Tseng YH, Dietrich DE, Ferziger JH (2005) Regional circulation of the Monterey Bay region: hydrostatic versus nonhydrostatic modeling. J Geophys Res Oceans 110(C9). https://doi.org/10.1029/2003JC002153

Tseng YH, Shen ML, Jan S, Dietrich DE, Chiang CP (2012) Validation of the Kuroshio current system in the dual-domain Pacific Ocean model framework. Prog Oceanogr 105:102–124

Tseng WL, Tsuang BJ, Keenlyside NS, Hsu HH, Tu CY (2015) Resolving the upper-ocean warm layer improves the simulation of the madden–Julian oscillation. Clim Dyn 44(5–6):1487–1503

Tsuang B-J, Tu C-Y, Arpe K (2001) Lake parameterization for climate models. Max-Planck-Institut für Meteorologie, Hamburg

Tsuang BJ, Tu CY, Tsai JL, Dracup JA, Arpe K, Meyers T (2009) A more accurate scheme for calculating Earth's skin temperature. Clim Dyn 32(2–3):251–272

Tu CY, Tsuang BJ (2005) Cool-skin simulation by a one-column ocean model. Geophys Res Lett 32(22)

Tudryn A, Chalié F, Lavrushin YA, Antipov MP, Spiridonova EA, Lavrushin V, Tucholka P, Leroy SAG (2013) Late quaternary Caspian Sea environment: late Khazarian and early Khvalynian transgressions from the lower reaches of the Volga river. Quat Int 292:193–204

Tudryn A, Leroy SAG, Toucanne S, Gibert-Brunet E, Tucholka P, Lavrushin YA, Dufaure O, Miska S, Bayon G (2016) The Ponto-Caspian basin as a final trap for southeastern Scandinavian ice-sheet meltwater. Quat Sci Rev 148:29–43

UNEP-Dewa (2003) Freshwater in Europe. Last accessed 25 March 2017

Van der Vorst HA (1992) Bi-CGSTAB: a fast and smoothly converging variant of Bi-CG for the solution of nonsymmetric linear systems. SIAM J Sci Stat Comput 13(2):631–644. https://doi.org/10.1137/0913035 https://en.wikipedia.org/wiki/Biconjugate_gradient_stabilized_method

Young CC, Tseng YH, Shen ML, Liang YC, Chen MH, Chien CH (2012) Software development of the Taiwan Multi-scale Community Ocean Model (TIMCOM). Environ Model Softw 38:214–219

Young CC, Liang YC, Tseng* YH, Chow CH (2014) Characteristics of the RAW filtered leapfrog time-stepping scheme in the ocean general circulation model. Mon Weather Rev 142:434–447